

Effect of Higher Order Chemical Reaction on Heat and Mass Transfer Analysis in Darcy-Forchheimer Flow of Hybrid Nanofluid over a Stretching Sheet

Puspanjali Mahapatra ¹ , Tusar Parida ^{1,2} , Kharabela Swain ^{2,*} 

¹ Department of Mathematics, Silicon University, Bhubaneswar-751024, India; math.22dmtl07@silicon.ac.in (P.M.); tusar.parida@silicon.ac.in (T.P.);

² Department of Mathematics, GIFT Autonomous, Bhubaneswar-752054, India; kharabelaswain@gift.edu.in;

* Correspondence: kharabelaswain@gift.edu.in;

Received: 4.10.2024; Accepted: 2.01.2025; Published: 25.11.2025

Abstract: The Darcy-Forchheimer model is used to investigate the flow, heat, and mass transfer of a hybrid nanofluid (HNF) over a stretching sheet in the presence of a magnetic field and a higher-order chemical reaction (HOCHR). The present model is used across many sectors, including biomedicine, microelectronics, biology, and industrial production processes. The nanoparticles (NPs), copper (metal), and titania (metallic oxide), along with water as a regular fluid, are considered. Copper NPs act as an antibacterial, antimicrobial, and antifungal agent, whereas titania NPs are used in the preparation of fabrics, windows, and anti-fogging automobile mirrors. It also acts as an environmental sanitizer. Similarity transformations convert the governing partial differential equations (PDEs) into a set of nonlinear ordinary differential equations (ODEs), which are then solved numerically using the bvp4c code. It is found that higher values of magnetic, Forchheimer, and slip parameters decrease the velocity profiles. The slip parameter and the chemical reaction parameter display opposite effects on the concentration profile. The volume fractions of NPs and the slip parameter have opposite effects on the skin friction coefficient and the Sherwood number.

Keywords: Darcy-Forchheimer flow; hybrid nanofluid; stretching sheet; magnetic field; higher-order chemical reaction.

© 2025 by the authors. This article is an open-access article distributed under the terms and conditions of the Creative Commons Attribution (CC BY) license (<https://creativecommons.org/licenses/by/4.0/>), which permits unrestricted use, distribution, and reproduction in any medium, provided the original work is properly cited. The authors retain copyright of their work, and no permission is required from the authors or the publisher to reuse or distribute this article, as long as proper attribution is given to the original source.

Nomenclature

x, y Cartesian coordinate system (m)	f Dimensionless velocity
u, v Velocity components along x, y directions respectively (m/s)	Re_x Local Reynolds number
a constant	Greek symbols
B_0 Magnetic field strength	θ Dimensionless temperature
C Concentration	λ Slip parameter
C_w Concentration at the sheet	ϕ Dimensionless nanoparticle volume fraction
C_∞ Ambient concentration	Φ Dimensionless concentration
Fr Forchheimer parameter	U_{hnf} Kinetic velocity of hybrid nanofluid (m ² /s)
M Magnetic parameter	U_f Kinetic velocity of base fluid (m ² /s)
Sc Schmidt number	σ_{hnf} Electrical conductivity of hybrid nanofluid ($\Omega^{-1}m^{-1}$)

x, y Cartesian coordinate system (m)	f Dimensionless velocity
C_b Forchheimer coefficient	σ_{nf} Electrical conductivity of nanofluid ($\Omega^{-1}m^{-1}$)
k_c chemical reaction coefficient	ρ_{hnf} Density of hybrid nanofluid (kg/m^3)
k_r chemical reaction parameter	ρ_{nf} Density of nanofluid (kg/m^3)
D_B Brownian motion coefficient (m^2/s)	ρ_f Density of base fluid (kg/m^3)
C_f Local skin friction coefficient	μ_{hnf} Viscosity of hybrid nanofluid ($kg/m\ s$)
Sh_x Local Sherwood number	μ_{nf} Viscosity of nanofluid ($kg/m\ s$)

1. Introduction

Hybrid nanofluid offers a wide range of industrial, biomedical, and engineering applications, such as the cosmetics industry, the automotive industry, cancer therapy, food packaging, fabrics, paper, plastics, paints, ceramics, food colourants, and soaps, due to higher thermal properties as compared to nanofluid (NF) and base fluid (BF). Nanotechnology used for advanced therapy and diagnostics has significant applications in medical sciences [1]. Hassanpour *et al.* [2] studied the biomedical applications of aluminium oxide NPs. Alghamdi *et al.* [3] investigate the delivery of HNF flow containing the medicine through blood vessels controlled by magnetic therapy. The influence of MHD flow on a blood-based hybrid nanofluid containing gold and copper nanoparticles in a stenosed artery, including viscous dissipation and Joule heating, has been examined by Imoro *et al.* [4].

The fluid flow and heat transfer past a stretched surface have many industrial applications, such as the cooling of metallic sheets, the production of glass fiber and paper, and metal and polymer extrusion processes. During these processes, a moving surface emerges from a slit, and as a result, a boundary-layer flow forms in the direction of the moving surface. The quality of the final product is significantly affected by the cooling rate. When two distinct NPs are dispersed in the base fluid, the result is an advanced NF called an HNF. HNF heat transfer research has attracted significant interest recently because it can transfer heat more quickly than conventional NF. Devi and Devi [5] investigated the flow of an HNF over a stretched surface while taking magnetic Cu-Al₂O₃ NPs into account. The effects of MWCNT and Fe₃O₄ NPs on an exponentially porous shrinking sheet with chemical reaction and slip boundary conditions were investigated by Swain *et al.* [6]. Waini *et al.* [7] investigated the HNF flow and heat transfer via a permeable stretching/shrinking surface with a convective boundary condition. Stability analysis of HNF flow over a stretching sheet was examined by Lund *et al.* [8]. Thumma *et al.* [9] considered the measurement of cupric oxide and silver NPs in the presence of the Coriolis force. Khashi'ie *et al.* [10] and Mishra *et al.* [11] studied HNF flow with the inclusion of Joule heating. Various flow models have been used by numerous authors to study the flow behaviour of NFs and HNFs [12–16].

Convective flow through porous media is used in a variety of environmental and industrial applications, including geophysics, design of heat exchangers, and catalytic reactors. The Darcy–Forchheimer (DF) model is a modification of linear Darcy's flow that accounts for similarity inertia effects by including a velocity-squared term in the momentum equation. Pal and Mondal [17] considered the non-Darcy Forchheimer's flow model on a stretched surface. In a thermally stratified medium, Anwar *et al.* [18] investigated the Darcy Forchheimer's flow across a moving vertical surface. Hayat *et al.* [19] quantitatively investigated the Darcy-

Forchheimer flow brought on by a curved stretching surface in the presence of homogeneous-heterogeneous processes. Vishnu Ganesh *et al.* [20] and Jawad *et al.* [21] examined the Darcy-Forchheimer flow across a porous stretched sheet. Padmaja and Rushi Kumar [22] considered higher-order chemical processes and Joule heating in the presence of a magnetic field. Recently, many authors [23-33] have studied the important physical parameters governing heat and mass transfer in NF and HNF flows, considering different flow geometries.

The slip-flow boundary condition is crucial for foams, suspensions, and polymer solutions. The no-slip border requirement is a factor in the aforementioned research. To the best of our knowledge, there is no study on the two-dimensional slip-flow of a hybrid nanofluid over a stretching sheet. The novelties of the present article are: (i) flow of hybrid nanofluid is considered, (ii) the effect of thermal radiation, higher order chemical reaction and magnetic field are taken into account, (iii) Darcy-Forchheimer flow is considered, (iv) Cu and TiO₂ nanoparticles for hybridization with base fluid (water), and (v) mono and hybrid nanofluid (HNF) flows are compared. This inspiration leads to examining the electromagnetic HNF flow past a stretched sheet in the presence of thermal radiation and higher-order chemical reactions. The similarity transformations reduced the PDEs to nonlinear ODEs, which were then solved numerically using the MATLAB *bvp4c* code. Graphical and tabular representations show the impact of different characterising physical parameters on the flow model.

This study is designed to answer the following important research questions: What are the consequences of the hybridization with copper and titania NPs on the thermophysical properties of the HNF model in the presence of Lorentz and inertial forces? What are the effects of electromagnetism, thermal radiation, and slip factors on the flow of HNF? How is mass transport influenced by higher-order chemical reactions and nanoparticle volume fraction?

2. Problem Formulation

The boundary layer MHD HNF flow past a stretching sheet is considered as shown in Figure 1, where x and y are Cartesian coordinates with x – the axis measured along the sheet and the y – axis normal to it. A constant magnetic field strength B_0 is applied in the direction of the y -axis. The sheet is stretched with a velocity $u_w(x) = ax$ where $a > 0$ is constant. The surface and ambient temperatures and concentrations are T_w and T_∞ , C_w and C_∞ respectively.

The assumptions incorporated for the simulations were:

The flow is in a two-dimensional steady state condition, and the hybrid nanofluid is incompressible.

The nanoparticles and the base fluid were in thermal equilibrium, and they had the same velocity.

The magnetic Reynolds number is assumed to be small, so the induced magnetic field is neglected.

Heat losses to the surroundings were negligible.

The thermo-physical properties of the hybrid nanofluid were constant and temperature-independent.

Using the above assumptions, the governing equations for steady flow of HNF following Ahmad *et al.* [34] are:

$$\frac{\partial u}{\partial x} + \frac{\partial u}{\partial y} = 0, \quad (1)$$

$$u \frac{\partial u}{\partial x} + v \frac{\partial u}{\partial y} = \nu_{hmf} \frac{\partial^2 u}{\partial y^2} - \frac{\sigma_{hmf}}{\rho_{hmf}} B_0^2 u - \frac{c_b}{\rho_{hmf} \sqrt{K}} u^2, \quad (2)$$

$$u \frac{\partial T}{\partial x} + v \frac{\partial T}{\partial y} = \frac{k_{hmf}}{(\rho C_p)_{hmf}} \frac{\partial^2 T}{\partial y^2} - \frac{1}{(\rho C_p)_{hmf}} \frac{\partial q_r}{\partial y}, \quad (3)$$

$$u \frac{\partial C}{\partial x} + v \frac{\partial C}{\partial y} = D_{hmf} \frac{\partial^2 C}{\partial y^2} - k_c (C - C_\infty)^n. \quad (4)$$

The prescribed boundary conditions are:

$$\left. \begin{aligned} \text{at } y = 0 : u = u_w(x) = ax + N \frac{\partial u}{\partial y}, v = 0, T = T_w, C = C_w, \\ \text{as } y \rightarrow \infty : u \rightarrow 0, T \rightarrow T_\infty, C \rightarrow C_\infty. \end{aligned} \right\} \quad (5)$$

Where u and v represent the velocity components of the HNF along the x -axes and y - axes, respectively, C denotes the HNF concentration. Further, μ_{hmf} , σ_{hmf} , and ρ_{hmf} are the dynamic viscosity, electrical conductivity, and density of the HNF, respectively. Table 1 provides the thermo-physical properties of NF and HNF. In Table 1, ϕ_1 and ϕ_2 are the volume fractions of Cu and Al_2O_3 NPs, respectively, where $\phi_1 = \phi_2 = 0$ represent the regular fluid, μ represents the dynamic viscosity, ρ is the density, and σ is the electrical conductivity, in which the subscripts $hmf, nf, f, n1$ and $n2$ represent HNF, NF, fluid, and solid components for Al_2O_3 and Cu NPs, respectively. Table 2 provides the physical properties of water Cu and Al_2O_3 NPs for a normal temperature of 298 K.

In order to convert the governing PDEs to non-linear ODEs, the following similarity variable and transformations are introduced.

$$u = axf'(\eta), v = -\sqrt{av_f} f(\eta), T = (T_w - T_\infty)\theta + T_\infty, C = (C_w - C_\infty)\Phi + C_\infty, \eta = y \sqrt{\frac{a}{\nu_f}}, \quad (6)$$

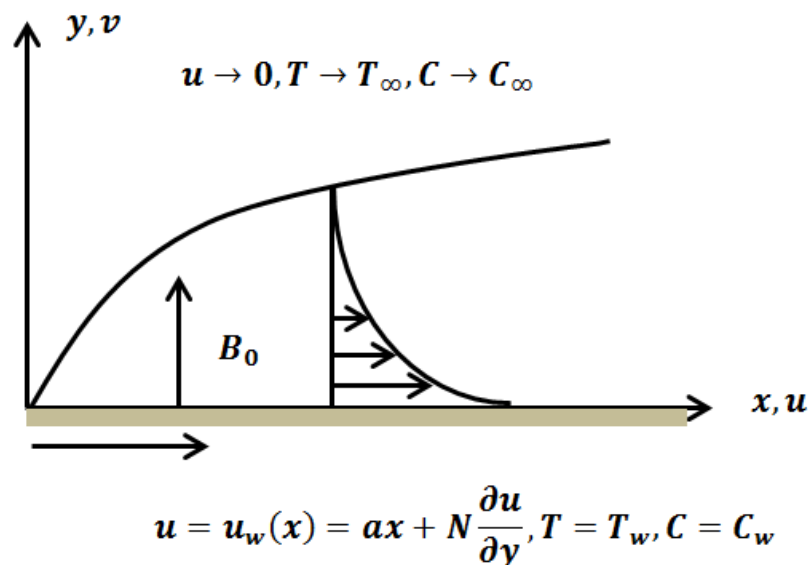


Figure 1. Flow configuration.

Using Eq. (6) in Eqs. (1) and (4), we get:

$$\frac{\mu_{hmf}/\mu_f}{\rho_{hmf}/\rho_f} f''' + ff'' - (1 + Fr) f'^2 - \frac{\sigma_{hmf}/\sigma_f}{\rho_{hmf}/\rho_f} Mf' = 0, \quad (7)$$

$$\frac{1}{(\rho C_p)_{hnf}/(\rho C_p)_f} \left(\frac{k_{hnf}}{k_f} + \frac{4}{3} R \right) \theta'' + Pr f \theta' = 0, \tag{8}$$

$$(1 - \phi_1)(1 - \phi_2) \Phi'' + Sc (f \Phi' - k_r \Phi^n) = 0, \tag{9}$$

and the boundary conditions (5) become:

$$\left. \begin{aligned} f(0) = 0, f'(0) = 1 + \lambda f'', \theta(0) = 1, \Phi(0) = 1, \\ f'(\infty) \rightarrow 0, \theta(\infty) \rightarrow 0, \Phi(\infty) \rightarrow 0. \end{aligned} \right\} \tag{10}$$

where $M = \frac{\sigma_f B_0^2}{\rho_f a}$, $Fr = \frac{c_b x}{\sqrt{K}}$, $\lambda = N \sqrt{\frac{a}{\nu_f}}$, $k_r = \frac{k_c}{a}$, $Pr = \frac{\nu_f}{\alpha_f}$ and $Sc = \frac{\nu_f}{D_B}$.

The skin friction coefficient (C_f), local Nusselt number (Nu_x), and local Sherwood number (Sh_x) are defined as $C_f = \frac{2\tau_w}{\rho_{hnf} u_w^2}$, $Nu_x = \frac{xq_w}{k_{hnf}(T_w - T_\infty)}$, $Sh_x = \frac{xq_m}{D_{hnf}(C_w - C_\infty)}$

respectively. Here τ_w , q_w and q_m denote the shear stress, heat flux and mass flux near the surface, and are given by $\tau_w = \mu_{hnf} \left(\frac{\partial u}{\partial y} \right)_{y=0}$, $q_w = -k_{hnf} \left(\frac{\partial T}{\partial y} \right)_{y=0} + (q_r)_{y=0} = 0$, and

$q_m = -D_{hnf} \left(\frac{\partial C}{\partial y} \right)_{y=0}$ respectively.

Finally, we get

$$Re_x^{1/2} C_f = \frac{\mu_{hnf}}{\mu_f} f''(0), Re_x^{-1/2} Nu_x = - \left(\frac{k_{hnf}}{k_f} + \frac{4}{3} R \right) \theta'(0), Re_x^{-1/2} Sh_x = -\Phi'(0)$$

where $Re_x = \frac{u_w x}{\nu_f}$ is the local Reynolds number.

Table 1. Thermophysical properties of NF and HNF (Gherasim *et al.* [35], Mintsa *et al.* [36]).

Properties	Nanofluid	Hybrid nanofluid
Density	$\rho_{nf} = (1 - \phi_1) \rho_f + \phi_1 \rho_{n1}$	$\rho_{hnf} = (1 - \phi_2) \rho_{nf} + \phi_2 \rho_{n2}$
Dynamic viscosity	$\mu_{nf} = \mu_f (0.904) e^{14.8\phi_1}$	$\mu_{hnf} = \mu_{nf} (0.904) e^{14.8\phi_2}$
Thermal conductivity	$k_{nf} = k_f (1 + 1.72\phi_1)$	$k_{hnf} = k_{nf} (1 + 1.72\phi_2)$
Heat capacity	$\frac{(\rho C_p)_{nf}}{(\rho C_p)_f} = (1 - \phi_1) + \phi_1 \frac{(\rho C_p)_{n1}}{(\rho C_p)_f}$	$\frac{(\rho C_p)_{hnf}}{(\rho C_p)_{nf}} = (1 - \phi_2) + \phi_2 \frac{(\rho C_p)_{n2}}{(\rho C_p)_{nf}}$
Electrical conductivity	$\frac{\sigma_{nf}}{\sigma_f} = 1 + \frac{3 \left(\frac{\sigma_{n1}}{\sigma_f} - 1 \right) \phi_1}{\frac{\sigma_{n1}}{\sigma_f} + 2 - \left(\frac{\sigma_{n1}}{\sigma_f} - 1 \right) \phi_1}$	$\frac{\sigma_{hnf}}{\sigma_{nf}} = 1 + \frac{3 \left(\frac{\sigma_{n2}}{\sigma_{nf}} - 1 \right) \phi_2}{\frac{\sigma_{n2}}{\sigma_{nf}} + 2 - \left(\frac{\sigma_{n2}}{\sigma_{nf}} - 1 \right) \phi_2}$

Table 2. Thermo-physical properties of water and NPs (see Yusuf *et al.* [37]).

Properties	$\rho(kg/m^3)$	$C_p(J/kgK)$	$k(W/mK)$	$\sigma(s/m)$
water	997.1	4179	0.613	5.5×10^{-6}
Cu	8933	385	400	5.96×10^7
TiO ₂	4250	686.2	8.9538	2.6×10^6

3. Results and Discussion

The current study investigates the steady 2D Darcy-Forchheimer HNF flow over a stretching sheet, accounting for magnetic field, thermal radiation, chemical reaction, and velocity slip. The magnetized fluid, in association with NPs such as metallic NP Copper (Cu) and metallic oxide NP titania (TiO₂) in the base fluid (water), exhibits these characteristics. The present results show a good agreement with the earlier works [38-41] and are presented in Tables 3 and 4. This supports both the current findings and the methodology's proposed convergence criterion. Additionally, we maintained the non-dimensional parameter values $M = Fr = 0.1, R = 0.3, n = 2, \lambda = k_r = 0.5, \phi_1 = \phi_2 = 0.05$ and $Sc = 2$ throughout the computation, unless otherwise stated in figures.

Table 3. Comparison of $f''(0)$ for different values of λ when $M = Fr = \phi_1 = \phi_2 = 0$.

λ	$f''(0)$		
	Sahoo and Do [38]	Tulu and Ibrahim [39]	Present study
0.0	1.001154	1.000000	1.002411
0.1	0.871447	0.872083	0.872083
0.2	0.774933	0.776377	0.776377
0.3	0.699738	0.701548	0.701548
0.5	0.589195	0.591196	0.591195
1.0	0.428450	0.430160	0.430158
2.0	0.282893	0.283981	0.283966
5.0	0.144430	0.144842	0.144798
10.0	0.081091	0.081245	0.081423
20.0	0.043748	0.043792	0.043774

Table 4. Comparison of $\theta'(0)$ different values of Pr when $M = Fr = R = \lambda = \phi_1 = \phi_2 = 0$.

Pr	$\theta'(0)$		
	Khan and Pop [40]	Yahya <i>et al.</i> [41]	Present study
2	0.9113	0.9112	0.90803
6.13	----	1.7597	1.75612
7	1.8954	1.8953	1.89187
20	3.3539	3.3540	3.35069

Figure 2 exhibits that the base fluid (BF) attains a minimum velocity compared to the nanofluid (NF) and hybrid nanofluid (HNF). It is also observed that metallic-based NF has a higher velocity than metallic-based NF. This is due to the addition of NPs to the BF. The TiO₂-based nanofluids were mostly used in turning and grinding operations. It is seen that velocity profiles decrease with higher values of the magnetic parameter (M), leading to a decrease in the velocity boundary layer thickness in the presence of slip (see Figure 3). Physically, the magnetic field produces a strong resistive force called the Lorentz force, which opposes the motion of the HNF. The same trend is also perceived for the slip parameter. Figure 4 shows that the velocity profiles decrease with moderate values of the Forchheimer parameter. This is due to the effect of the inertial force, which drags the fluid backward and thus decreases its motion. It is evident from the velocity profile. Figure 5 shows that temperature increases with increasing values of the thermal radiation parameter.

Figure 6 shows the impact of the slip parameter and the Prandtl number on the temperature distribution. The temperature of the HNF increases with increasing values of the slip parameter and Prandtl number.

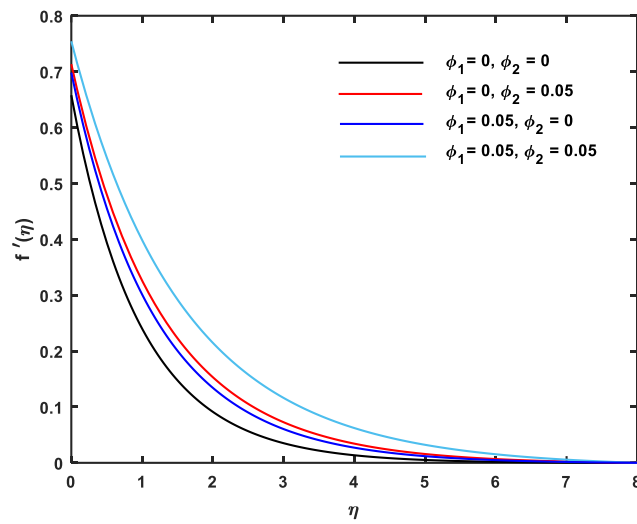


Figure 2. Velocity distribution for different volume fractions of nanoparticles.

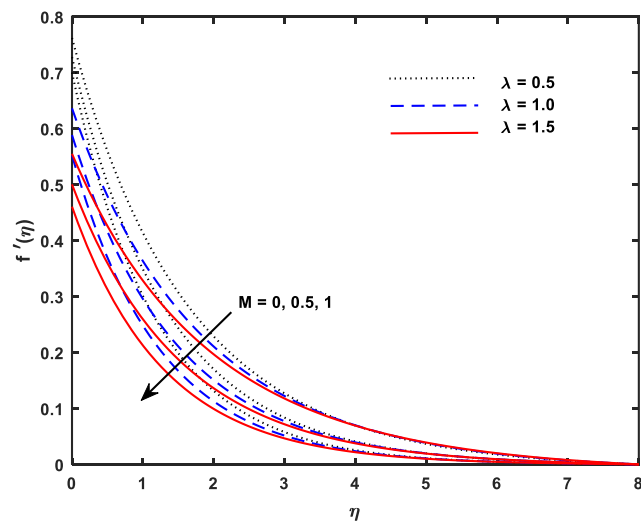


Figure 3. Velocity distribution for various values of M and λ .

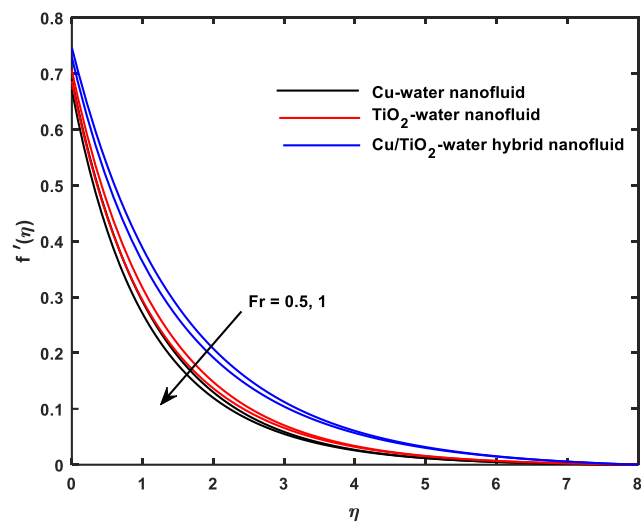


Figure 4. Velocity distribution for various values of Fr .

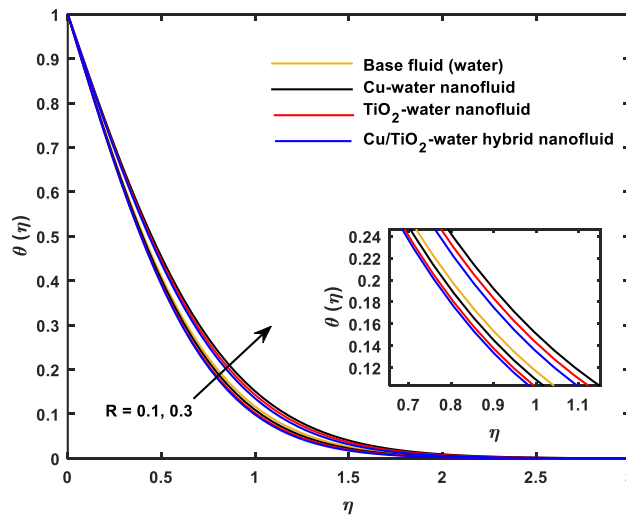


Figure 5. Temperature distribution for various values of R .

Figure 7 shows that higher values of Schmidt number (Sc) lead to a reduction in the concentration profiles, as Sc is the ratio of momentum diffusivity and mass diffusivity. Further, it is seen that the concentrations of HNF, NF, and the base fluid are almost the same in the presence of a chemical reaction, but in its absence, a lower concentration is observed for HNF. Figure 8 shows that increasing values of the chemical reaction parameter uniformly decrease the concentration profiles. It may occur because chemical reactions enhance the rate of mass transfer and reduce the solutal boundary layer thickness. Here $k_r > 0$ relates to a constructive chemical reaction.

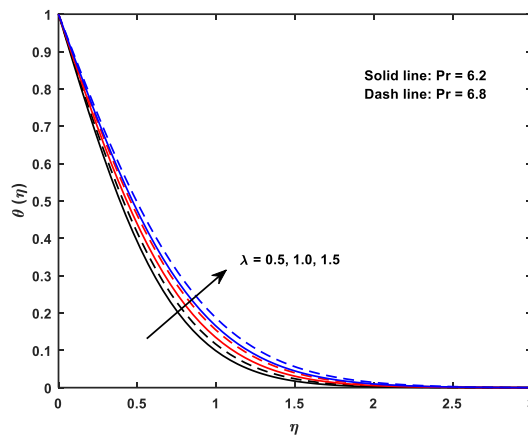


Figure 6. Temperature distribution for various values of λ and Pr .

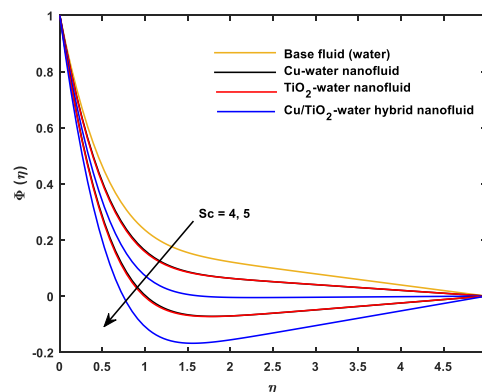


Figure 7. Concentration distribution for various values of Sc .

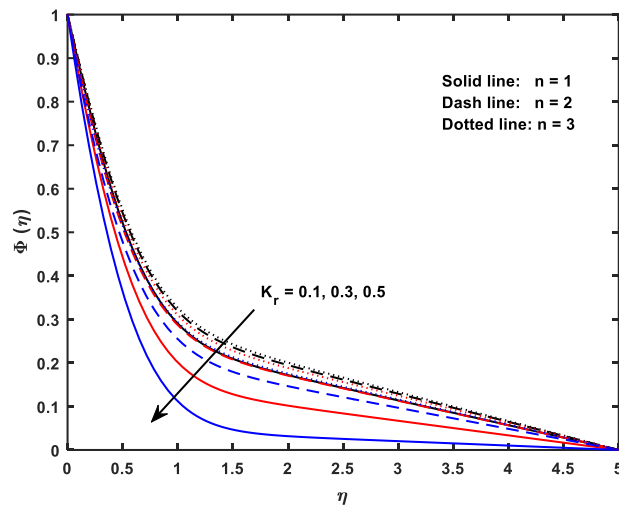


Figure 8. Concentration distribution for various values of k_r and n .

Table 5 reveals that a higher volume fraction of NPs is favourable to increase the magnitude of the skin friction coefficient ($f''(0)$), Nusselt number ($-\theta'(0)$), and Sherwood number ($-\Phi'(0)$), but the opposite effect is observed in the case of the slip parameter. The magnetic and Forchheimer parameters are responsible for decreasing $f''(0)$ and increasing the rate of heat and mass transfer. Further, constructive chemical reaction ($k_r > 0$) parameters and destructive chemical reactions ($k_r < 0$) have opposite effects on the mass transfer rate at the surface. The slower rate of mass transfer is caused by a higher-order chemical reaction.

Table 5. Computational values of $f''(0)$, $\theta'(0)$ and $-\Phi'(0)$ when $R = 0.3, Sc = 2, Pr = 6.8$.

ϕ_1	ϕ_2	M	Fr	λ	n	k_r	$f''(0)$	$-\theta'(0)$	$-\Phi'(0)$
0	0	0.1	0.1	0.5	2	0.1	-0.543616	1.710653	0.680348
0.03							-0.788537	1.797404	0.719828
0.05							-1.003198	1.858442	0.748629
	0.03						-1.386672	1.970504	0.801324
	0.05						-1.715136	2.040692	0.837412
		0.5					-1.911398	1.966541	0.815091
		1.0					-2.115418	1.885534	0.790940
			0.5				-2.190597	1.858066	0.782791
			1.0				-2.275025	1.826816	0.773556
				1.0			-1.669521	1.599552	0.707064
				1.5			-1.328591	1.444978	0.663413
				0			-3.738493	2.238675	0.898698
				0.5	3		-2.275025	1.826816	0.754130
					5		-2.275025	1.826816	0.736523
					1		-2.275025	1.826816	0.821410
					2	0.5	-2.275025	1.826816	1.051186
						1.0	-2.275025	1.826816	1.398222
						0	-2.275025	1.826816	0.704149
						-0.5	-2.275025	1.826816	0.357113
						-1.0	-2.275025	1.826816	0.010076

4. Conclusion

The numerical treatment of the Darcy-Forchheimer HNF flow past a stretched sheet, influenced by a magnetic field, thermal radiation, and a higher-order chemical reaction, is presented. The characteristics of the physical parameters are depicted through graphs and tabular form. It is found that higher values of magnetic, Forchheimer, and slip parameters decrease the velocity profiles. The temperature of HNF is an increasing function of the slip and chemical reaction parameters. The concentration profile is an increasing function of the slip parameter and the chemical reaction parameter. The presence of heavier species in the flow field (higher Sc) decreases the concentration in the boundary layer. Schmidt number and chemical reaction parameter enhance the rate of mass transfer. The volume fractions of NPs and the slip parameter have opposite effects on the skin friction coefficient and the Sherwood number.

Author Contributions

Conceptualization, P.M., T.P., and K.S.; methodology, P.M., T.P., and K.S.; software, K.S.; validation, K.S.; formal analysis, P.M., T.P., and K.S.; investigation, P.M., T.P., and K.S.; resources, P.M., T.P., and K.S.; data curation, P.M., T.P., and K.S.; writing—original draft preparation, P.M., T.P., and K.S.; writing—review and editing, K.S.; visualization, P.M., T.P., and K.S.; supervision, T.P. and K.S. All authors have read and agreed to the published version of the manuscript. All authors must confirm their agreement with the contribution statement before submission.

Institutional Review Board Statement

Not applicable.

Informed Consent Statement

Not applicable.

Data Availability Statement

Data supporting the findings of this study are available upon reasonable request from the corresponding author.

Funding

This research received no external funding.

Acknowledgments

The authors thank Prof. G. C. Dash for his valuable suggestions and timely help in improving the quality of the paper.

Conflicts of Interest

The authors declare no conflict of interest.

References

1. Godin, B.; Sakamoto, J.H.; Serda, R.E.; Grattoni, A.; Bouamrani, A.; Ferrari, M. Emerging applications of nanomedicine for the diagnosis and treatment of cardiovascular diseases. *Trends in Pharmacological Sciences* **2010**, *31*, 199-205, <https://doi.org/10.1016/j.tips.2010.01.003>.
2. Hassanpour, P.; Panahi, Y.; Ebrahimi-Kalan, A.; Akbarzadeh, A.; Davaran, S.; Nasibova, A.N.; Khalilov, R.; Kavetsky, T. Biomedical applications of aluminium oxide NPs. *Micro Nano Letters* **2018**, *13*, 1227-1231, <https://doi.org/10.1049/mnl.2018.5070>.
3. Alghamdi, W.; Alsubie, A.; Kumam, P.; Saeed, A.; Gul, T. MHD HNF flow comprising the medication through a blood artery. *Sci. Rep.* **2021**, *11*, 1-13, <https://doi.org/10.1038/s41598-021-91183-6>.
4. Imoro, I.; John Etwire, C.; Musah, R. MHD flow of blood-based hybrid nanofluid through a stenosed artery with thermal radiation effect. *Case Studies in Thermal Engineering* **2024**, *59*, 104418, <https://doi.org/10.1016/j.csite.2024.104418>.
5. Devi, S.P.A.; Devi, S.S.U. Numerical investigation of hydromagnetic hybrid Cu-Al₂O₃/water NF flow over a permeable stretching sheet with suction. *Int. J. Nonlinear Sci. Numer. Simul.* **2016**, *17*, 249-257, <https://doi.org/10.1515/ijnsns-2016-0037>.
6. Swain, K.; Mebarek-Oudina, F.; Abo-Dahab, S.M. Influence of MWCNT/ Fe₃O₄ hybrid NPs on an exponentially porous shrinking sheet with chemical reaction and slip boundary conditions. *J Therm Anal Calorim* **2022**, *147*, 1561-1570, <https://doi.org/10.1007/s10973-020-10432-4>.
7. Waini, I.; Ishak, A.; Pop, I. Hybrid nanofluid flow and heat transfer past a permeable stretching/shrinking surface with a convective boundary condition. *J. Phys.: Conf. Ser.* **2019**, *1366*, 012022, <https://doi.org/10.1088/1742-6596/1366/1/012022>.
8. Lund, L.A.; Omar, Z.; Khan, I.; Sherif El-Sayed, M. Dual Solutions and Stability Analysis of a Hybrid Nanofluid over a Stretching/Shrinking Sheet Executing MHD Flow. *Symmetry* **2020**, *12*, 276, <https://doi.org/10.3390/sym12020276>.
9. Thumma, T.; Ahammad, N.A.; Swain, K.; Animasuan, I.L.; Mishra, S.R. Increasing effects of Coriolis force on the cupric oxide and silver nanoparticles based nanofluid flow when thermal radiation and heat source/sink are significant. *Waves in Random and Complex Media* **2025**, *35*, 1333-1350, <https://doi.org/10.1080/17455030.2022.2032471>.
10. Khashi'ie, N.S.; Arifin, N.M.; Pop, I. Magnetohydrodynamics (MHD) boundary layer flow of HNF over a moving plate with Joule heating. *Alexandria Eng. J.* **2022**, *61*, 1938-1945, <https://doi.org/10.1016/j.aej.2021.07.032>.
11. Mishra, S.; Swain, K.; Dalai, R. Joule Heating and Viscous Dissipation Effects on Heat Transfer of Hybrid Nanofluids with Thermal Slip. *Iran J Sci Technol Trans Mech Eng.* **2024**, *48*, 531-539, <https://doi.org/10.1007/s40997-023-00681-7>.
12. Zeeshan; Ahammad, A.; Shah, N.A.; Dong Chung, J. Role of Nanofluid and Hybrid Nanofluid for Enhancing Thermal Conductivity towards Exponentially Stretching Curve with Modified Fourier Law Inspired by Melting Heat Effect. *Mathematics* **2023**, *11*, 1170, <https://doi.org/10.3390/math11051170>.
13. Zainodin, S.; Jamaludin, A.; Nazar, R.; Pop, I. Effects of higher order chemical reaction and slip conditions on mixed convection hybrid ferrofluid flow in a Darcy porous medium. *Alexandria Eng. J.* **2023**, *68*, 111-126, <https://doi.org/10.1016/j.aej.2023.01.011>.
14. Basavarajappa, M.; Muhammad, T.; Lorenzini, G.; Swain, K. Darcy–Forchheimer Nanoliquid Flow and Radiative Heat Transport over Convectively Heated Surface with Chemical Reaction. *J. Engin. Thermophys.* **2022**, *31*, 261-273, <https://doi.org/10.1134/S1810232822020072>.
15. Biswal, M.M.; Swain, K.; Dash, G.C.; Mishra, S. Study of chemically reactive and thermally radiative Casson NF flow past a stretching sheet with a heat source. *Heat Transfer* **2023**, *52*, 333-353, <https://doi.org/10.1002/hjt.22697>.
16. Swain, K.; Mishra, M.; Abha Kumari. Numerical study of Casson nanofluid over an elongated surface in presence of Joule heating and viscous dissipation: Buongiorno model analysis. *Journal of Computational Applied Mechanics* **2022**, *53*, 414-430, <https://doi.org/10.22059/JCAMECH.2022.347011.745>.
17. Pal, D.; Mondal, H. Effects of Soret, Dufour, chemical reaction and thermal radiation on MHD non-Darcy unsteady mixed convective heat and mass transfer over a stretching sheet. *Commun Nonlinear Sci Numer Simulat* **2011**, *16*, 1942-1958, <https://doi.org/10.1016/j.cnsns.2010.08.033>.

18. Beg O. Anwar; Zueco, J.; Takhar, H.S. Laminar free convection from a continuously-moving vertical surface in thermally-stratified non Darcian high-porosity medium: network numerical study. *Int Commun Heat Mass Transfer* **2008**, *35*, 810-816, <https://doi.org/10.1016/j.icheatmasstransfer.2008.03.007>.
19. Joshi, N.; Upreti, H.; Pandey, A.K. MHD Darcy-Forchheimer Cu-Ag/H₂O-C₂H₆O₂ hybrid nanofluid flow via a porous stretching sheet with suction/blowing and viscous dissipation. *International Journal for Computational Methods in Engineering Science and Mechanics* **2022**, *23*, 527-535, <https://doi.org/10.1080/15502287.2022.2030426>.
20. Vishnu Ganesh, N.; Abdul Hakeema, A.K.; Ganga, B. Darcy-Forchheimer flow of hydromagnetic nanofluid over a stretching/shrinking sheet in a thermally stratified porous medium with second order slip, viscous and Ohmic dissipations effects. *Ain Shams Engineering Journal* **2018**, *9*, 939-951, <https://doi.org/10.1016/j.asej.2016.04.019>.
21. Jawad, M.; Hameed, M.K.; Nisar, K.S.; Majeed, A.H. Darcy-Forchheimer flow of maxwell nanofluid flow over a porous stretching sheet with Arrhenius activation energy and niel boundary conditions. *Case Studies in Thermal Engineering* **2023**, *44*, 102830, <https://doi.org/10.1016/j.csite.2023.102830>.
22. Padmaja, K.; Rushi Kumar, B. Higher order chemical reaction effects on Cu-H₂O nanofluid flow over a vertical plate. *Sci. Rep.* **2022**, *12*, 17000, <https://doi.org/10.1038/s41598-022-20155-1>.
23. Md. Fayz-Al-Asad; Mebarek-Oudina, F.; Vaidya, H.; Md. Shamim Hasan; Md. Manirul Alam Sarker; Ismail, A. I. Finite Element Analysis for Magneto-convection Heat Transfer Performance in Vertical Wavy Surface Enclosure: Fin Size Impact. *Frontiers in Heat and Mass Transfer* **2024**, *22*, 817-837, <https://doi.org/10.32604/fhmt.2024.050814>.
24. Anil kumar, M.; Mebarek-Oudina, F.; Mangathai, P.; Shah, N.A.; Ch. Vijayabhaskar; Venkatesh, N.; Fouad, Y. The Impact of Soret Dufour and Radiation on the Laminar Flow of a Rotating liquid past a Porous plate via Chemical Reaction. *Modern Physics Letters B* **2024**, *39*, 2450458, <https://doi.org/10.1142/S021798492450458X>.
25. Dharmaiiah, G.; Mebarek-Oudina, F.; Balamurugan, K.S.; Vedavathi, N. Numerical Analysis of the Magnetic Dipole Effect on a Radiative Ferromagnetic Liquid Flowing over a Porous Stretched Sheet. *Fluid Dyn. Mater. Process* **2024**, *20*, 293-310, <https://doi.org/10.32604/fdmp.2023.030325>.
26. Mebarek-Oudina, F.; Chabani, I.; Vaidya, H.; Ismail, A.I. Hybrid nanofluid magneto-convective flow and porous media contribution to entropy generation. *International Journal of Numerical Methods for Heat & Fluid Flow* **2024**, *34*, 809-836, <https://doi.org/10.1108/HFF-06-2023-0326>.
27. Ramesh, K.; Mebarek-Oudina, F.; Ismail, A.I.; Jaiswal, B.R.; Warke, A.S.; Lodhi, R.K.; Sharma, T. Computational analysis on radiative non-Newtonian Carreau nanofluid flow in a microchannel under the magnetic properties. *Scientia Iranica* **2023**, *30*, 376-390, <https://doi.org/10.24200/sci.2022.58629.5822>.
28. Dharmaiiah, G.; Mebarek-Oudina, F.; Rama Prasad, J.L.; Ch. Baby Rani. Exploration of Bio-convection for slippery two-phase Maxwell Nanofluid past a vertical induced magnetic stretching regime associated for Biotechnology and Engineering. *Journal of Molecular Liquids* **2023**, *391*, 123408, <https://doi.org/10.1016/j.molliq.2023.123408>.
29. Mebarek-Oudina, F.; Dharmaiiah, G.; Balamurugan, K.S.; Ismail, A.I.; Saxena, H. The Role of Quadratic-Linearly Radiating Heat Source with Carreau Nanofluid and Exponential Space-Dependent Past a Cone and a Wedge: A Medical Engineering Application and Renewable Energy. *Journal of Computational Biophysics and Chemistry* **2023**, *22*, 997-1011, <https://doi.org/10.1142/S2737416523420073>.
30. Chandini Pattanaik, P.; Jena, S.; Mishra, S.R. Control of magnetic dissipation and radiation on an unsteady stagnation point nanofluid flow: A numerical approach. *Modern Physics Letters B* **2024**, *38*, 2450039, <https://doi.org/10.1142/S0217984924500398>.
31. Pattnaik, P.K.; Mishra, S.; Baitharu, A.P.; Jena, S. Cu-kerosene and Al₂O₃-kerosene boundary layer nanofluid flow past a stretching/shrinking surface. *Proceedings of the Institution of Mechanical Engineers, Part N: Journal of Nanomaterials, Nanoengineering and Nanosystems* **2023**, *237*, 75-81, <https://doi.org/10.1177/23977914221103986>.
32. Bhukta, D.; Dash, G.C.; Mishra, S.R.; Jena, S. Analytical estimation of energy dissipations: Viscous, Joulian, and Darcy of viscoelastic fluid flow phenomena over a deformable surface. *Heat Transf.* **2021**, *50*, 7798-7816, <https://doi.org/10.1002/htj.22254>.
33. Acharya, S.; Nayak, B.; Mishra, S.R.; Jena, S. Adomian decomposition method for the MHD flow of a viscous fluid with the influence of dissipative heat energy. *Heat Transf.* **2020**, *49*, 4612-4625, <https://doi.org/10.1002/htj.21844>.

34. Ahmad, S.; Ali, K.; Rizwan, W.; Ashraf, M. Heat and mass transfer attributes of copper aluminum oxide hybrid NPs flow through a porous medium. *Case Studies in Thermal Engineering* **2021**, *25*, 100932, <https://doi.org/10.1016/j.csite.2021.100932>.
35. Gherasim, I.; Roy, G.; Nguyen, C.T.; Vo-Ngoc, D. Experimental investigation of nanofluids in confined laminar radial flows. *Int J Therm Sci.* **2009**, *48*, 1486-1493, <https://doi.org/10.1016/j.ijthermalsci.2009.01.008>.
36. Mintsu, H.A.; Roy, G.; Nguyen, C.T.; Doucet, D. New temperature dependent thermal conductivity data for water-based nanofluids. *Int J Therm Sci.* **2009**, *48*, 363-371, <https://doi.org/10.1016/j.ijthermalsci.2008.03.009>.
37. Yusuf, T.A.; Mabood, F.; Khan, W.A.; Gbadeyan, J.A. Irreversibility analysis of Cu-TiO₂-H₂O hybrid-nanofluid impinging on a 3-D stretching sheet in a porous medium with nonlinear radiation: Darcy-Forchheimer's model. *Alexandria Eng. J.* **2020**, *59*, 5247-5261, <https://doi.org/10.1016/j.aej.2020.09.053>.
38. Sahoo, B.; Do, Y. Effects of slip on sheet-driven flow and heat transfer of a third grade fluid past a stretching sheet. *International Communications in Heat and Mass Transfer* **2010**, *37*, 1064-1071, <https://doi.org/10.1016/j.icheatmasstransfer.2010.06.018>.
39. Tulu, A.; Ibrahim, W. Effects of Second-Order Slip Flow and Variable Viscosity on Natural Convection Flow of (CNTs – Fe₃O₄)/Water Hybrid Nanofluids due to Stretching Surface. *Mathematical Problems in Engineering* **2021**, *2021*, 8407194, <https://doi.org/10.1155/2021/8407194>.
40. Khan, W.A.; Pop, I. Boundary-layer flow of a nanofluid past a stretching sheet. *International Journal of Heat and Mass Transfer* **2010**, *53*, 2477-2483, <https://doi.org/10.1016/j.ijheatmasstransfer.2010.01.032>.
41. Yahya, A.U.; Salamat, N.; Wen-Hua Huang; Siddique, I.; Abdal, S.; Hussain, S. Thermal characteristics for the flow of Williamson hybrid nanofluid (MoS₂ + ZnO) based with engine oil over a stretched sheet. *Case Studies in Thermal Engineering* **2021**, *26*, 101196, <https://doi.org/10.1016/j.csite.2021.101196>.

Publisher's Note & Disclaimer

The statements, opinions, and data presented in this publication are solely those of the individual author(s) and contributor(s) and do not necessarily reflect the views of the publisher and/or the editor(s). The publisher and/or the editor(s) disclaim any responsibility for the accuracy, completeness, or reliability of the content. Neither the publisher nor the editor(s) assume any legal liability for any errors, omissions, or consequences arising from the use of the information presented in this publication. Furthermore, the publisher and/or the editor(s) disclaim any liability for any injury, damage, or loss to persons or property that may result from the use of any ideas, methods, instructions, or products mentioned in the content. Readers are encouraged to independently verify any information before relying on it, and the publisher assumes no responsibility for any consequences arising from the use of materials contained in this publication.